

BEARING FAULT DETECTION BY FOUR-BAND WAVELET PACKET DECOMPOSITION

by

Yalcin CEKIC

Mechatronics Program, Vocational School of Bahcesehir University Istanbul, Istanbul, Turkey

Original scientific paper
<https://doi.org/10.2298/TSCI180927333C>

Bearing problems are by far the biggest cause of induction motor failures in the industry. Since induction machines are used heavily by the industry, their unexpected failure may disturb the production process. Motor condition monitoring is employed widely to avoid such unexpected failures. The data that can be obtained from induction machines are non-stationary by nature since the loading may vary during their operation. Wavelet packet decomposition seems to better handle non-stationary nature of induction machines, the use of this method in monitoring applications is limited, since the computational complexity is higher than other methods. In this work four-band wavelet packet decomposition of motor vibration data is proposed to reduce the computational complexity without compromising accuracy. The proposed method is very suitable for parallel computational processing by its nature, and as a result it is predicted that the calculation time will be shortened further if field-programmable gate array is used in design.

Key words: *bearing fault detection, four-band wavelet packet decomposition, computational complexity*

Introduction

Induction motors are used widely in both industrial and residential environments due to their low cost, ruggedness, and easy maintenance. Any interruption to their continued operation may be costly financially. Therefore, condition monitoring and preventive maintenance of such motors is so vital. Sound [1], thermal [2-4], vibration [1, 5], and current signature analysis [6] are some of the methods used in motor condition monitoring and preventive maintenance. Vibration analysis is the most effective approach in detecting the mechanical faults such as bearing problems since the fault related signals are directly obtained by placing vibration transducers in proper locations. The accessibility was the main shortcoming of this approach but recently this limitation is lifted with the introduction of wireless vibration sensor arrays [7, 8].

Fourier analysis, enveloping, and wavelet decomposition are used in the analysis of vibration data [9, 10]. The motor speed and mechanical fault related frequencies vary with changes in load levels. As a result, the motor fault related frequencies are non-stationary in nature. Wavelet decomposition is the most appropriate technique among the aforementioned analysis tools for non-stationary signal analysis. The wavelet packet decomposition has a higher computational complexity than some of the alternative analysis techniques limiting its use in some environments. In order to overcome this limitation caused by increased computational

cost, four-band wavelet packet decomposition is used in motor current signature analysis [11, 12]. In this study, the use of modified four-band wavelet filter bank structure and different observation windows are proposed to achieve fault detection using vibration data with reduced computational complexity. The proposed method does not compromise the detection accuracy.

Motor fault types and characteristic vibration frequencies

The induction motor faults are caused by internal or external sources. External sources can be divided in three groups [13]: electrical (transient voltage, unbalanced voltage, voltage fluctuations), environmental (humidity, temperature, cleanliness), and mechanical (over load, poor mounting, pulsating load). On the other hand, internal sources can be divided in two groups: electrical and mechanical stresses [5].

There are many reasons for bearing faults (previously mentioned): the most important are manufacturing errors, improper assembly, loading, operation, lubrication, and fatigue of the bearing material [14]. When the spectrum of a healthy and new bearing is examined, it will be seen that the vibration of it is very small and looks like random noise. With the start of the fault, the vibration generated by the bearing also starts to change. When a rolling-element pass a discontinuity in its path a vibration will occur as a result. The vibration caused by the discontinuities is in the form of pulses. When the vibration is inspected it is seen to be periodic and the period is determined by the bearing geometry, such as: pitch diameter, ball diameter, number of balls and contact angle, and by the location of the discontinuity [14]. A regular ball bearing geometry is given in fig. 1.

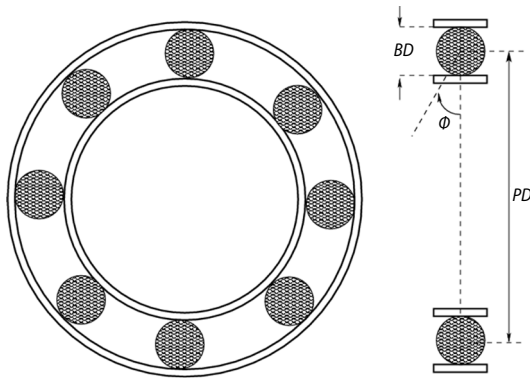


Figure 1. A regular bearing geometry
 Φ – contact angle, PD – the pitch diameter, and BD – the ball diameter

frequency outer-race (BPFO) for a fault on the outer-race, and the ball-spin frequency (BSF) for a fault on the ball. Depending on the rotational speed and bearing geometry these frequencies can be calculated using the equations:

- Outer race defect frequency:

$$f_{\text{BPFO}} = \frac{n}{2} f_r \left(1 - \frac{BD}{PD} \cos \Phi \right) \quad (1)$$

- Inner race defect frequency:

$$f_{\text{BPFI}} = \frac{n}{2} f_r \left(1 + \frac{BD}{PD} \cos \Phi \right) \quad (2)$$

- Ball defective frequency:

$$f_{\text{BSF}} = \frac{PD}{2BD} f_r \left[1 - \left(\frac{BD}{PD} \cos \Phi \right)^2 \right] \quad (3)$$

In the literature these rates are known as the frequency of bearing or bearing frequencies. These frequencies are: the fundamental train frequency (FTF) for a fault on the cage, the ball-passing frequency inner-race (BPFI) for a fault on the inner-race, the ball-passing

frequency outer-race (BPFO) for a fault on the outer-race, and the ball-spin frequency (BSF) for a fault on the ball.

– Cage defect frequency:

$$f_{\text{FTF}} = \frac{1}{2} \left(1 - \frac{BD}{PD} \cos \Phi \right) \quad (4)$$

where n is a number of balls and f_r [Hz] is a shaft frequency.

Multi-band wavelet decomposition

There are many transforms for testing finite-energy, periodic, discrete-time signals and the most widely used ones are Fourier based transforms. Practically, discrete Fourier transform (DFT) is still used for the vibration analysis of bearings under steady-state condition since the periodicity depends to the geometry and rotational speed of the bearing. It is possible to determine vibration components with reasonable accuracy. On the other hand, if there are speed fluctuations because of changing load levels, bearing fault frequency detection in the spectra using classical DFT methods is difficult. As a relatively new tool wavelet analysis has been used in signal processing applications such as object recognition [15], data compression [16], video and image processing [17, 18]. There are some works to determine the bearing faults using wavelet transform [19, 20]. The continuous wavelet transform of a finite energy signal, $s(t)$, with the analyzing wavelet, $\psi(t)$, is the convolution of $s(t)$ with a scaled and conjugated wavelet:

$$W(a, b) = a^{-\frac{1}{2}} \int_{-\infty}^{+\infty} s(t) \psi^* \left(\frac{t-b}{a} \right) dt \quad (5)$$

where $\psi(t)$ is the wavelet function, and $W(a, b)$ measures the similarity between the signal, $s(t)$, and the analyzing wavelet, $\psi(t)$, at different scales as defined by the parameter a , and different time positions as defined by the parameter b . The $a^{-1/2}$ is used for energy preservation. Equation (5) shows that that the wavelet analysis is a time-frequency analysis, or, more properly termed, a time-scale analysis. The wavelet transform can be also considered as a special filtering operation. The frequency segmentation is obtained by translation and dilation of the analyzing wavelet. The discrete wavelet transform is performed by choosing fixed values $a = 2^m$ and $b = n2^m$, where m and n are integer values. Thus, discrete wavelets $\psi_{m,n}(t) = 2^{-m/2} \psi(2^{-m}t - n)$ can be constructed, which can also constitute an orthonormal basis. The discrete wavelet analysis can be implemented by the scaling filter, $h(n)$, which is a low-pass filter related to the scaling function, $\phi(t)$, and the wavelet filter, $g(n)$, which is a high-pass filter related to the wavelet function, $\psi(t)$:

$$h(n) = \frac{1}{\sqrt{2}} \langle \phi(t), \phi(2t - n) \rangle \quad (6)$$

$$g(n) = \frac{1}{\sqrt{2}} \langle \psi(t), \psi(2t - n) \rangle = (-1)^n h(1 - n) \quad (7)$$

The basic step of a fast wavelet algorithm is illustrated in fig. 2 and can be implemented iteratively in signal decomposition. In the decomposition step, the discrete signal s is convolved with a low-pass filter, H_0 , and a high-pass filter, H_1 , resulting in two vectors $cA1$ and $cD1$. The elements of the vector $cA1$ are called approximation coefficients, and the ele-

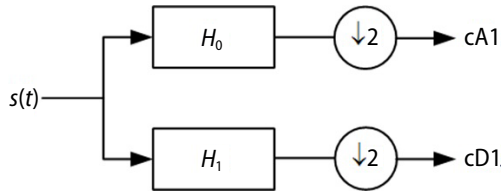


Figure 2. Basic step of wavelet decomposition

ments of vector $cD1$ are called detailed coefficients. The symbol $\downarrow 2$ denotes down sampling.

The M -band wavelet decomposition is a direct generalization of the previous two-band case [21, 22]. Let $\phi(x)$ be the scaling function satisfying:

$$\phi(x) = \sum_K h(k) \sqrt{M} \phi(Mx - k) \tag{8}$$

In addition, there are $M - 1$ wavelets which also satisfy:

$$\psi^j(x) = \sum_k \sqrt{M} h^{(j)} \psi(Mx - k) \tag{9}$$

Equations (10) and (11) represents scaling function and $M - 1$ wavelets in discrete form, respectively:

$$\phi_{ik}(x) = \sum_K M^{-i/2} \phi(M^{-i}x - k) \tag{10}$$

$$\psi_{ik}^j(x) = \sum_k M^{-\frac{i}{2}} \psi^{(j)} \psi(M^{-i}x - k), \quad j = 1, 2, 3, \dots, M - 1 \tag{11}$$

There is close relation between the M channel filters and M -band wavelets [23]. In M channel filter bank the bandwidth of filter is divided into M bands as shown in fig. 3(a). Figure 3(b) shows the four-level decomposition of 1-D signal using M band wavelet transform for $M = 4$. The vibration data is decomposed by four-band wavelets in this study to provide reduction in computational complexity. Here, $H_0(z)$ is a low-pass, $H_1(z)$, and $H_2(z)$ are band-pass, and $H_3(z)$ is a high-pass filters, respectively. During the implementation stage of this four band analysis filter, polyphase decomposition is used for finite impulse response (FIR) filter realization. In the general case, an M -branch polyphase decomposition of the transfer function ($H[z] = \sum_{k=0}^N h[k]z^{-k}$), a causal FIR filter of order N is of the form:

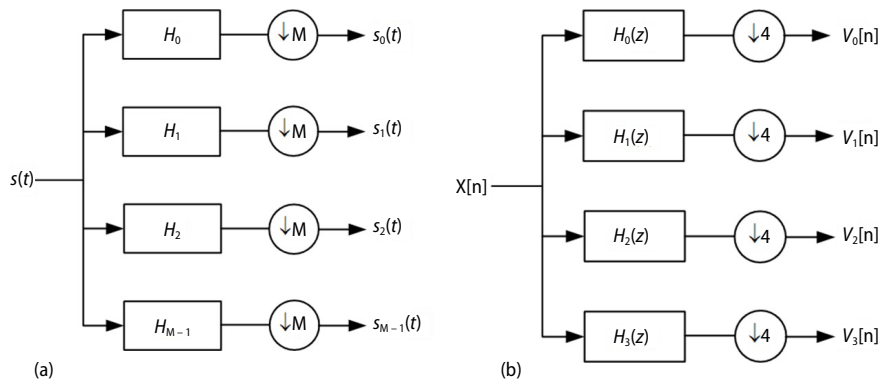


Figure 3. (a) M channel analysis filter bank (b) four-band ($M = 4$) analysis filter bank

$$H[z] = \sum_{k=0}^{M-1} z^{-k} E_k(z^M) \quad (12)$$

where

$$E_k(z) = \sum_{n=0}^{\text{floor}\{(N+1)/M\}} h[Mn+k]z^{-n}, \quad 0 \leq k \leq M-1 \quad (13)$$

with $h[n] = 0$ for $n > N$. The $H[z]$ becomes:

$$H[z] = E_0(z^4) + z^{-1}E_1(z^4) + z^{-2}E_2(z^4) + z^{-3}E_3(z^4) \quad (14)$$

for four-branch polyphase.

The overall decimator implementation of the filter bank is indicated in fig. 4(a), whereas computationally more efficient structure of fig. 4(b).

Let the low-pass prototype transfer function:

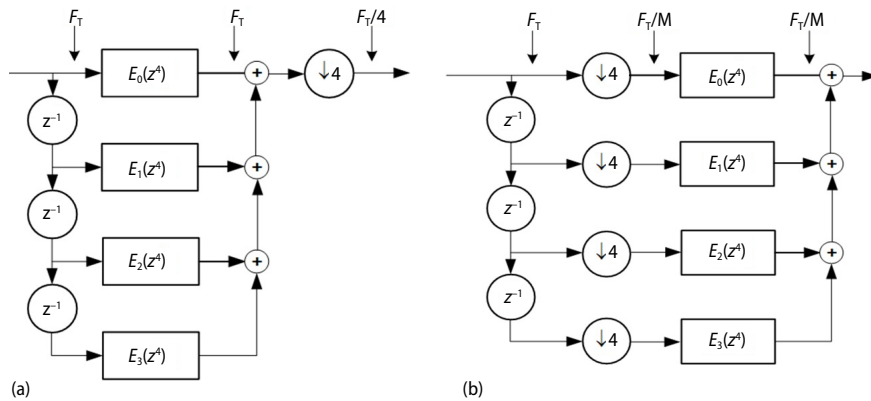


Figure 4. (a) Decimator implementation based on Type I polyphase decomposition and (b) computationally efficient decimator structure ($M = 4$)

$$H_0(z) = \sum_{\ell=0}^{M-1} z^{-\ell} E_{\ell}(z^M) \quad (15)$$

where $E_{\ell}(z)$ is the ℓ^{th} polyphase component of $H_0(z)$:

$$E_{\ell}(z) = \sum_{n=0}^{\infty} e_{\ell}(n)z^{-n} = \sum_{n=0}^{\infty} h_0(\ell + nM)z^{-n}, \quad 0 \leq \ell \leq M-1 \quad (16)$$

Substituting z with zW_M^k in eq. (15) we arrive at the M -band polyphase decomposition of $H_k(z)$:

$$H_k(z) = \sum_{\ell=0}^{M-1} z^{-\ell} W_M^{-k\ell} E_{\ell}(z^M) \quad (17)$$

where $W_M = e^{-j2\pi/M}$, and $W_M^{kM} = 1$ identity is used. Equation (17) can be written in matrix form:

$$H_k(z) = \begin{bmatrix} 1 & W_M^{-k} & W_M^{-2k} & \dots & W_M^{-(M-1)k} \end{bmatrix} \begin{bmatrix} z^0 & 0 & 0 & 0 \\ 0 & z^{-1} & 0 & 0 \\ 0 & 0 & \ddots & 0 \\ 0 & 0 & 0 & z^{-(M-1)} \end{bmatrix} \begin{bmatrix} E_0(z^M) \\ E_1(z^M) \\ \vdots \\ E_{M-1}(z^M) \end{bmatrix} \quad (18)$$

where $0 \leq k \leq M-1$.

For $M=4$ eq. (18) becomes:

$$\begin{bmatrix} H_0(z) \\ H_1(z) \\ H_2(z) \\ H_3(z) \end{bmatrix} = \begin{bmatrix} 1 & 1 & 1 & 1 \\ 1 & j & -1 & -j \\ 1 & -1 & 1 & -1 \\ 1 & -j & -1 & j \end{bmatrix} \begin{bmatrix} E_0(z^4) \\ E_1(z^4) \\ E_2(z^4) \\ E_3(z^4) \end{bmatrix} \quad (19)$$

In this work, a low-pass prototype FIR filter is used with order 55 ($N=55$). Magnitude responses (dB) of polyphase filters (dB) are given, fig. 5.

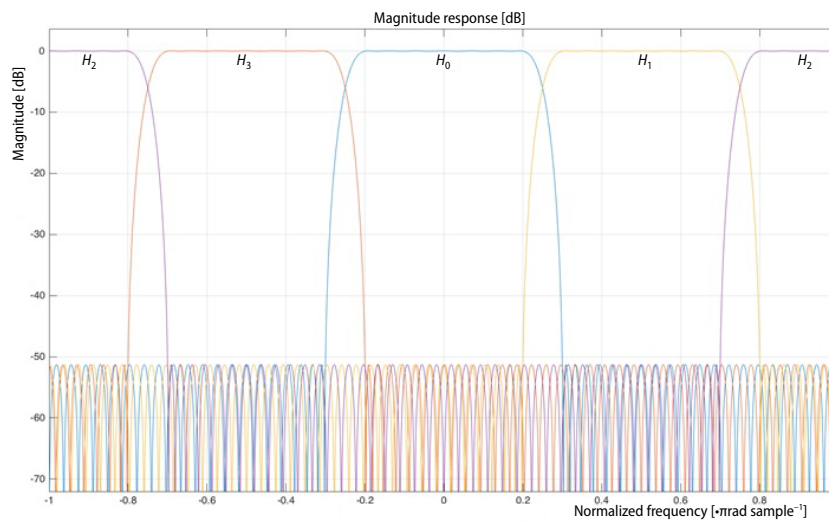


Figure 5. Four channel uniform DFT analysis filter bank
(for color image see journal web site)

Test results

The test set-up consists of a three-phase one horsepower squirrel cage induction machine and a Fuko break as the load. The front-end (rotor side) bearing is 6205 2ZC3 whereas the rear-end bearing is 6004 2ZC3. The front-end bearing was tested in this study. The test data is collected by National Instruments data acquisition card from a vibration transducer at sampling rate of 12.8 kHz for a second. The vibration transducer is mounted on the motor case and is perpendicular to the bearing. The vibration data collected from the motor front-end bearing is displayed in fig. 6. In each case data for ten runs are collected.

The front-end bearing cage is dented slightly to create a cage defect. The motor is run at full load with the Fuko break and the rated speed is around 1450 rpm when operated with the line frequency of 50 Hz. The cage defect vibration frequency is calculated using eq. (4) since

we also know the bearing geometry. The fundamental defect frequency is around 10 Hz and the integer multiples of it are the harmonics. The first two harmonic frequencies (10 and 20 Hz) are explored in this study.

In testing, the collected vibration data is decomposed into four bands and passed through four stages of filter banks.

The wavelet coefficients for the lowest frequency band in last three stages are depicted in fig. 7.

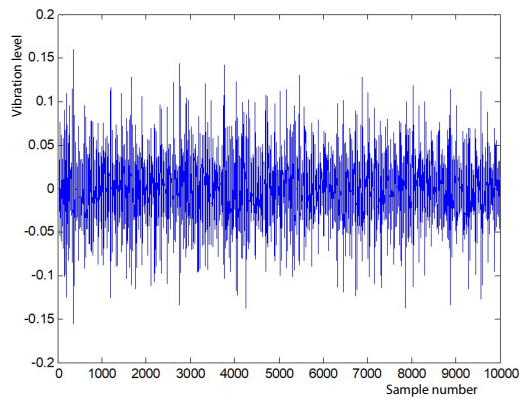


Figure 6. Bearing vibration data

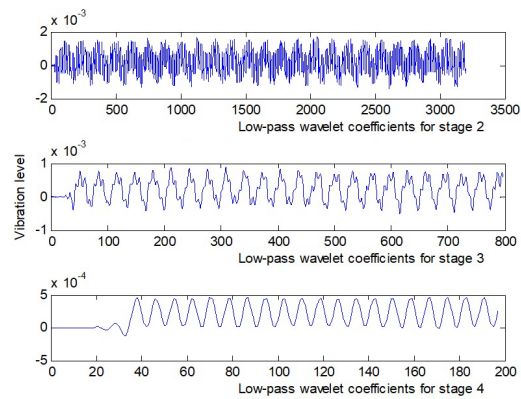


Figure 7. Output of lowest frequency band at last three stages

At the last level 25Hz bandwidth is achieved from such decomposition. Consequently, the lowest frequency band has 0 to 25 Hz range covering the first two cage related fault frequency harmonics. The energy level of the low-pass wavelet coefficients are calculated using root mean squares. The average and standard deviation values for ten trials of each case are given in tab. 1. The data indicates significant increase (about 70%) in energy levels for the associated frequency band in the case of a bearing with a faulty cage.

The computational complexity of a typical two-band (half-band) decomposition with widely used Daubechies (db18) filter banks can be compared with the proposed four-band decomposition by looking at the number of multiplications required for a full decomposition. The number of multiplications required to fully decomposing motor vibration data of 12800 points into four levels with db18 FIR half-band and a four-band filters are given in tab. 2. The data indicates that the proposed approach results in a lower computational complexity than commonly used half-band FIR filters without a compromise in fault detection accuracy.

There is a significant reduction in the number of serial multiplications required for the proposed method. Here, the use of parallel processing with an FPGA implementation would improve the time performance even further as indicated in the tab. 2.

Table 1. Cage defect

	Average	Std deviation
Healthy cage	$3.30 \cdot 10^{-3}$	$0.16 \cdot 10^{-3}$
Faulty cage	$5.61 \cdot 10^{-3}$	$0.09 \cdot 10^{-3}$

Table 2. Computational complexity

	Serial	Parallel
Daubechies half-band	$3.686 \cdot 10^6$	$1.843 \cdot 10^6$
Proposed four-band	$2.867 \cdot 10^6$	$0.717 \cdot 10^6$

Conclusion

In this study, the bearing vibration data is analyzed by four-band wavelet packet decomposition to detect bearing faults. The proposed algorithm detects bearing faults with a better

computational complexity than commonly used half-band decomposition algorithms. The proposed algorithm has a higher level of parallel processing and it can provide better time performance if implemented on an FPGA system.

References

- [1] Williams, K., *et al.*, Vibrations of Long and Short Laminated Stators of Electrical Machines Part II: Results For Long Stators, *J. Sound Vib.*, 129 (1989), 1, pp. 15-29
- [2] Bonnett, A. H., Soukup, G. C., Cause And Analysis Of Stator And Rotor Failures in Three-Phase Squirrel-Cage Induction Motors, *IEEE Trans. Ind. Appl.*, 28 (1992), 4, pp. 921-937
- [3] Bonnett, A. H., Soukup, G. C., Rotor Failures in Squirrel Cage Induction Motors, *IEEE Trans. Ind. Appl.*, IA-22 (1986), 6, pp. 1165-1173
- [4] Klimenta, D. O., Hannukainen, A., Novel Approach to Analytical Modelling of Steady-State Heat Transfer from the Exterior of TEFC Induction Motors, *Thermal Science*, 21 (2017), 3, pp. 1529-1542
- [5] Bianchini, C., *et al.*, Fault Detection of Linear Bearings in Brushless AC Linear Motors by Vibration Analysis, *IEEE Trans. Ind. Electron.*, 58 (2011), 5, pp. 1684-1694
- [6] Schoen, R. R., *et al.*, Motor Bearing Damage Detection Using Stator Current Monitoring, *IEEE Trans. Ind. Appl.*, 31 (1995), 6, pp. 1274-1279
- [7] Xiong, X., *et al.*, Vibration Monitoring System of Ships Using Wireless Sensor Networks, *Proceedings, Mechatronics and Automation (ICMA)*, 2014 IEEE International Conference on Mechatronics and Automation, Tianjin, China, 2014, pp. 90-94
- [8] Ramalingam, I., *et al.*, Fault Diagnosis of Wind Turbine Bearing Using Wireless Sensor Networks, *Thermal Science*, 21 (2017), Suppl. 2, pp. S523-S531
- [9] Prabhakar, S., *et al.*, Application of Discrete Wavelet Transform for Detection of Ball Bearing Race Faults, *Tribol. Int.*, 35 (2002), 12, pp. 793-800
- [10] Betta, G., *et al.*, A DSP-Based FFT-Analyzer for the Fault Diagnosis of Rotating Machine Based on Vibration Analysis, *IEEE Trans. Instrum. Meas.*, 51 (2002), 6, pp. 1316-1322
- [11] Eren, L., *et al.*, Computational Complexity of Four-Band Wavelet Packet Decomposition in Motor Fault Diagnostics, *J. Trends Dev. Mach.*, 19 (2015), 1, pp. 97-100
- [12] Cekic, Y., Eren, L., Broken Rotor Bar Detection Via Four-Band Wavelet Packet Decomposition Of Motor Current, *Electr. Eng.*, 100 (2018), 3, pp. 1957-1962
- [13] Bhowmik, P. S., *et al.*, Fault Diagnostic and Monitoring Methods of Induction Motor: A Review, *Int. J. Appl. Control.*, 1 (2013), 1, pp. 1-18
- [14] ***, Bruel&Kjaer, Application note, Detecting Faulty Rolling Element Bearings, http://www.bkvb.com/fileadmin/mediapool/Internet/Application_Notes/detecting_faulty_rolling_element_bearings.pdf
- [15] Guo, Y., *et al.*, 3D Object Recognition in Cluttered Scenes with Local Surface Features: A Survey, *IEEE Trans. Pattern Anal. Mach. Intell.*, 36 (2014), 11, pp. 2270-2287
- [16] Littler, T. B., Morrow, D. J., Wavelets for the Analysis and Compression of Power System Disturbances, *IEEE Trans. Power Deliv.*, 14 (1999), 2, pp. 358-364
- [17] Shen, K., Delp, E. J., Wavelet Based Rate Scalable Video Compression, *Circuits Syst. Video Technol. IEEE Trans.*, 9 (1999), 1, pp. 109-122
- [18] Antonini, M., *et al.*, Image Coding Using Wavelet Transform., *IEEE Trans. Image Process.*, 1 (1992), 2, pp. 205-220
- [19] Eren, L., Devaney, M. J., Bearing Damage Detection Via Wavelet Packet Decomposition of the Stator Current, *IEEE Trans. Instrum. Meas.*, 53 (2004), 2, pp. 431-436
- [20] Teotrakool, K., *et al.*, Adjustable-Speed Drive Bearing-Fault Detection Via Wavelet Packet Decomposition, *IEEE Trans. Instrum. Meas.*, 58 (2009), 8, pp. 2747-2754
- [21] Steffen, P., *et al.*, Theory of Regular M-Band Wavelet Bases, *IEEE Trans. Signal Process.*, 41 (1993), 12, pp. 3497-3511
- [22] Acharyya, M., Kundu, M. K., An Adaptive Approach to Unsupervised Texture Segmentation Using M-Band Wavelet Transform, *Signal Processing*, 81 (2001), 7, pp. 1337-1356
- [23] Gopinath, R. A., Burrus, C. S., Wavelets And Filter Banks, in: *Wavelets: A Tutorial in Theory and Applications*, Academic Press, San Diego, Cal., USA, 1992, pp. 603-654